DOE F 241.3
(2-01) p.1 of 2

UNITED STATES DEPARTMENT OF ENERGY (DOE)
Announcement of Scientific and Technical Information (STI)
(For Use By Financial Assistance Recipients and Non-M&O/M&I Contractors)

OMB CONTROL NO. 1910-1400

PART I: STI PRODUCT DESCRIPTION
(To be completed by Recipient/Contractor)

A. STI Product Identifiers
1. REPORT/PRODUCT NUMBER(s)
None
2. DOE AWARD/CONTRACT NUMBER(s)
DE-FC36-97ID13554
3. OTHER IDENTIFYING NUMBER(s)
None

B. Recipient/Contractor
Carnegie Mellon University, Dept. of Materials Science and Engineering, 5000 Forbes Ave., Pittsburgh, PA 15213

C. STI Product Title
Clean Steel: Advancing the State of the Art

D. Author(s)
Sridhar Seetharaman
Alan W. Cramb

E-mail Address(es):
Sridhar@andrew.cmu.edu

E. STI Product Issue Date/Date of Publication
05 19 2004
MM DD YYYY

F. STI Product Type (*Select only one*)
☒ 1. TECHNICAL REPORT
☒ *Final* ☐ *Other (specify)* _____

☐ 2. CONFERENCE PAPER/PROCEEDINGS
Conference Information (title, location, dates)

☐ 3. JOURNAL ARTICLE
a. TYPE: ☐ *Announcement Citation Only* ☐ *Preprint* ☐ *Postprint*
b. JOURNAL NAME
c. VOLUME _____ *d. ISSUE* _____
e. SERIAL IDENTIFIER (e.g. ISSN or CODEN)

☐ 4. OTHER, SPECIFY

G. STI Product Reporting Period
11 01 2001 Thru 03 31 2004
MM DD YYYY MM DD YYYY

H. Sponsoring DOE Program Office
Office of Industrial Technologies (OIT)(EE20)

I. Subject Categories *(list primary one first)*
32 Energy Conservation, Consumption and Utilization
Keywords: Steel

J. Description/Abstract
The project had 3 objectives: (1) to determine the kinetic factors governing inclusion removal from liquid steel at the slag metal interface, (2) to develop a methodology to enable steels of less than 1 ppm total oxygen to be produced with an average inclusion diameter of less than 5 um, and (3) to determine the slag-metal interface conditions necessary for ultra clean steels.

K. Intellectual Property/Distribution Limitations
(must select at least one; if uncertain contact your Contracting Officer (CO))
☒ 1. UNLIMITED ANNOUNCEMENT *(available to U.S. and non-U.S. public; the Government assumes no liability for disclosure of such data)*
☐ 2. COPYRIGHTED MATERIAL: *Are there any restrictions based on copyright?* ☐ *Yes* ☐ *No.*
If yes, list the restrictions as contained in your award document
☐ 3. PATENTABLE MATERIAL: THERE IS PATENTABLE MATERIAL IN THE DOCUMENT.
INENTION DISCLOSURE SUBMITTED TO DOE:
DOE Docket Number: S-
(Sections are marked as restricted distribution pursuant to 35 USC 205)
☐ 4. PROTECTED DATA: ☐ CRADA ☐ *Other, specify*
Release date (required) no more than 5 years from date listed in Part I.E. above ___ ___ ____ (MM DD YYYY)
☐ 5. SMALL BUSINESS INNOVATION RESEARCH (SBIR) DATA
Release date (required) no more than 4 years from date listed in Part I.E. above ___ ___ ____ (MM DD YYYY)
☐ 6. SMALL BUSINESS TECHNOLOGY TRANSFER RESEARCH (STTR) DATA
Release date (required) no more than 4 years from date listed in Part I.E. above ___ ___ ____ (MM DD YYYY)
☐ 7. OFFICE OF NUCLEAR ENERGY APPLICED TECHNOLOGY

L. Recipient/Contract Point of Contact *Contact for additional information (contact or organization name To be included in published citations and who would Receive any external questions about the content of the STI Product or the research contained herein)*
Dr. Sridhar Seetharaman
Name and/or Position
Sridhar@andrew.cmu.edu (412) 268-2675
E-mail *Phone*
Dept. of Mat'l Science and Engineering, Carnegie Mellon University, Pittsburgh, PA 15213

UNITED STATES DEPARTMENT OF ENERGY (DOE)
Announcement of Scientific and Technical Information (STI)
(For Use By Financial Assistance Recipients and Non-M&O/M&I Contractors)

OMB CONTROL NO.
1910-1400

PART II: STI PRODUCT MEDIA/FORMAT and LOCATION/TRANSMISSION

(To be completed by Recipient/Contractor)

A. Media/Format Information:

1. MEDIUM OF STI PRODUCT IS:
   ☒ Electronic Document ☐ Computer Medium
   ☐ Audiovisual Material ☒ Paper ☐ No Full-text
2. SIZE OF STI PRODUCT 37 Pages
3. SPECIFY FILE FORMAT OF ELECTRONIC DOCUMENT BEING TRANSMITTED, INDICATE:
   ☐ SGML ☐ HTML ☐ XML ☒ PDF Normal
   ☐ PDF Image ☐ TIFFG4
   ☐ WP-indicate Version (*5.0 or greater)* _____
   Platform/operation system _____
   ☐ MS-indicate Version (*5.0 or greater)* _____
   Platform/operation system _____
   ☐ Postscript _____
4. IF COMPUTER MEDIUM OR AUDIOVISUAL MATERIAL:
   a. Quantity/type (*specify)* _____
   b. Machine compatibility (*specify)* _____
   c. Other information about product format a user needs to know:
   _____

B. Transmission Information:

1. STI PRODUCT IS BEING TRANSMITTED:
   ☒ a. Electronically via E-Link
   b. Via mail or shipment to address indicated in award document (*Paper product, CD-ROM, diskettes, video cassettes, etc.)*
   _____
2. INFORMATION PRODUCT FILE NAME
   ☒ *(of transmitted electronic format)*
   EditedTRP0003FinalReport.

PART III: STI PRODUCT REVIEW/RELEASE INFORMATION

(To be completed by DOE)

A. STI Product Reporting Requirements Review.

☐ 1. THIS DELIVERABLE COMPLETES ALL REQUIRED DELIVERABLES FOR THIS AWARD
☐ 2. THIS DELIVERABLE FULFILLS A TECHNICAL INFORMATION REPORTING REQUIREMENT, BUT SHOULD NOT BE DISSEMINATED BEYOND DOE.

B. Award Office Is the Source of STI Product Availability

☐ THE STI PRODUCT IS NOT AVAILABLE IN AN ELECTRONIC MEDIUM. THE AWARDING OFFICE WILL SERVE AS THE INTERIM SOURCE OF AVAILABILITY.

C. DOE Releasing Official

☐ 1. I VERIFY THAT ALL NECESSARY REVIEWS HAVE BEEN COMPLETED AS DESCRIBED IN DOE G 241.1-1A, PART II, SECTION 3.0 AND THAT THE STI PRODUCT SHOULD BE RELEASED IN ACCORDANCE WITH THE INTELLECTUAL PROPERTY/DISTRIBUTION LIMITATION ABOVE.

Release by (*name)* _____

Date ___ ___ _____
MM DD YYYY

E-Mail _____

Phone _____

AISI/DOE Technology Roadmap Program

Final Report

TRP 0003 - Clean Steel: Advancing the State of the Art

by

Sridhar Seetharaman

and

Alan W. Cramb

May 19, 2004

Work Performed under Cooperative Agreement
No. DE-FC36-97ID13554

Prepared for
U.S. Department of Energy

Prepared by
American Iron and Steel Institute
Technology Roadmap Program Office
Pittsburgh, PA 15222

Title and Subtitle

AISI/DOE Manufacturing and Technology Program
TRP 0003 - Clean Steel: Advancing the State of the Art

Authors

Sridhar Seetharaman
Alan W. Cramb

Performing Organization

Carnegie Mellon University
Department of Materials Science and Engineering
5000 Forbes Avenue
Pittsburgh
PA 15213

Abstract

This project had 3 objectives: (1) to determine the kinetic factors governing inclusion removal from liquid steels at a slag metal interface; (2) to develop a methodology to enable steels of less than 1 ppm total oxygen to be produced with an average inclusion diameter of less than 5 μm; and, (3) to determine the slag-metal interface conditions necessary for ultra clean steels. In objectives 1, and 3, the major finding was that dissolution rates of solid particles in slags were found to be significant in both ladle and tundish slags and must be included in a model to predict steel cleanliness. The work towards objective 2 indicated that liquid steel temperature was a very significant factor in our understanding of clean steel potential and that undercooled steels equilibrated with low oxygen potential inert gases have the potential to be significantly cleaner than current steels. Other work indicated that solidification front velocity could be used to push particles to produce clean steels and that reoxidation must be severely curtailed to allow the potential for clean steels to be realized.

DISCLAIMER

"This report was prepared as an account of work sponsored by an Agency of the United States Government. Neither the United States Government nor any agency thereof, nor any of their employees, makes any warranty, express or implied, or assumes any legal liability or responsibility for the accuracy, completeness, or usefulness of any information, apparatus, product, or process disclosed, or represents that its use would not infringe privately owned rights. Reference herein to any specific commercial product, process, or service by trade name, trademark, manufacturer, or otherwise, does not necessarily constitute or imply endorsement, recommendation, or favoring by the United States Government or any agency thereof. The views and opinions of authors expressed herein do not necessarily state or reflect those of the United States Government or any agency thereof."

"This report has been reproduced from the best available copy. Available in paper copy and microfiche"

Number of pages in report: 37

DOE and DOE contractors can obtain copies of this report
FROM: Office of Scientific and Technical Information, P.O. Box 62, Oak Ridge, TN 37831. (615)576-8401

This report is publicly available from the Department of Commerce, National Technical Information Service, 5285 Port Royal Road, Springfield, VA 22161. (703) 487-4650.

TABLE OF CONTENTS

LIST OF FIGURES

LIST OF TABLES

TRP 0003 - Clean Steel: Advancing the State of the Art

Final Project Report

by

Y. Wang, M. E. Valdez, S. Sridhar and A. W. Cramb

Introduction

The research in this project was aimed at elucidating the factors that control inclusion formation and removal of both solid and liquid inclusions from liquid steels. The findings of this research will be used to determine the types of slags and interfacial conditions that are necessary to ensure complete separation of inclusions from steels at a slag-metal interface and to determine the conditions that can lead to the formation of larger inclusions in steels. Direct observation of phenomena at high temperatures was necessary and Confocal Scanning Microscopy was used to elucidate the mechanisms responsible for inclusion agglomeration and removal.

The objectives of the project were:

- To determine the kinetic factors governing inclusion removal from liquid steels at a slag-metal interface;
- To develop a methodology to enable steels of less than 1 ppm total oxygen to be produced with an average inclusion diameter of less than 5 microns;
- To determine the slag-metal interface conditions necessary for ultra clean steels.

The plan for the project followed the objectives outlined above:

1. Determine the factors controlling solid inclusion separation at a slag-metal interface
2. Determine the factors controlling liquid inclusion separation and agglomeration at a slag-metal interface
3. Determine the factors controlling particle dissolution rate as a function of slag composition
4. Develop an understanding of inclusion morphology during reoxidation with an oxidizing gas for various steel chemistries
5. Develop an understanding of the formation and separation of $MgO\text{-}Al_2O_3$ inclusions at a slag-metal interface
6. Develop an understanding of inclusion evolution during solidification.

The purpose of this final report is to document the work that was done to achieve the above objectives.

Major Findings and Work Completed

***Objective 1*: To determine the kinetic factors governing inclusion removal from liquid steels at a slag-metal interface**

The major findings of this part of the work were that inclusion dissolution times in liquid slags are significant and a function of slag chemistry and temperature. Although the fact that slag chemistry and temperature were well recognized as important before this work, the details of the relationship between these factors were not well documented. Thus a major issue in the removal of inclusions from a slag-metal interface is to dissolve the particle into a liquid slag.

Inclusion dissolution inside slags is essentially a solid/fluid reaction process as shown schematically in **Figure 1** below.

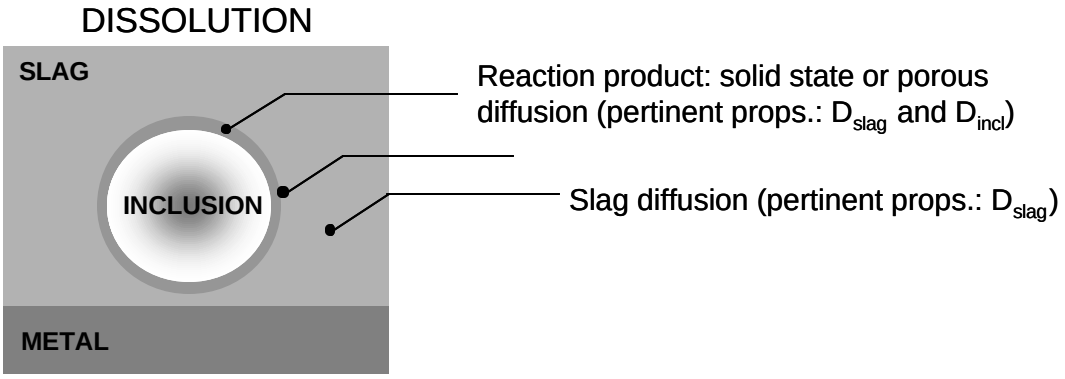

Figure 1: Schematic of the fluid/solid reaction of inclusion dissolution in slags.

High temperature Confocal Scanning Laser Microscopy was used to study the dissolution of: (i) Al_2O_3, MgO and $MgAl_2O_4$ in a 36%CaO-21%Al_2O_3-42%SiO_2 (mass contents in %) slag and (ii) Al_2O_3 in a high SiO_2 tundish slag and ladle slag. A schematic of the experimental assembly inside the hot-stage is shown in **Figure 2**.

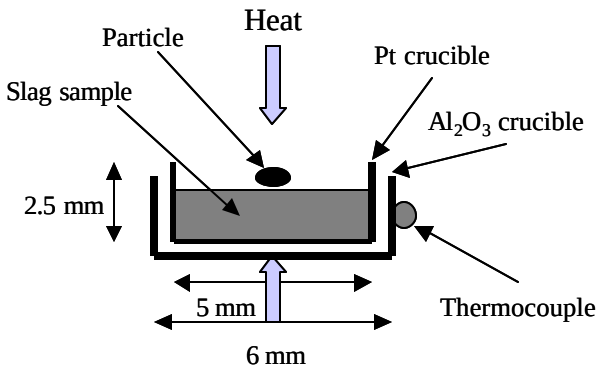

Figure 2: Schematic of Confocal Microscopy Experiment.

As the slag melted, the inclusions would settle towards the crucible bottom and the change in shape was observed through the microscope. Picture of a particle dissolving in a slag is given in **Figure 3**. It can be seen in this picture that the particles can be clearly observed leading to accurate measurement of dissolution rate.

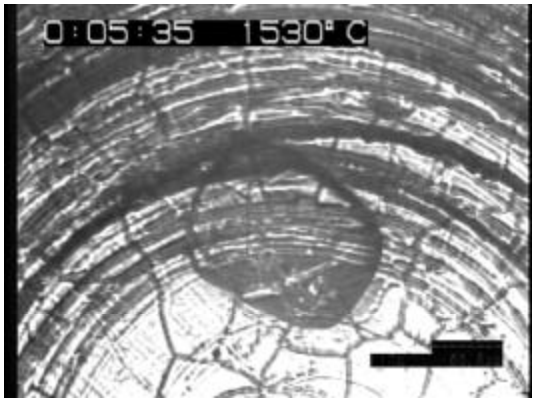

Figure 3: Appearance of an MgO particle being dissolved in a slag.

The dissolution time is a strong function of size as seen in **Figure 4** where MgO particle dissolution times are seen to vary by temperature and size. It can be seen that particles with a radius over 100 microns take a significant time (more than 100 seconds) to dissolve.

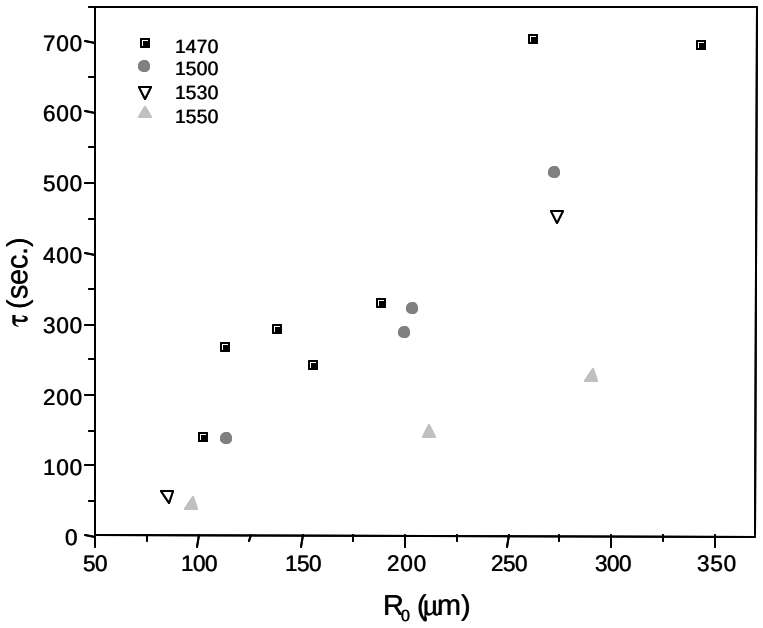

Figure 4: Typical dissolution time for MgO particles in a lime-alumina-silica slag.

In the case of the 36%CaO-21%Al_2O_3-42%SiO_2 slag it was observed that during the dissolution of MgO particles, a dark spinel layer (confirmed through SEM analysis) covered the particles. The resulting dissolution mechanism was found to lie between those of Al_2O_3 and $MgAl_2O_4$ dissolution and appeared to follow the boundary layer diffusion mechanism. The total dissolution times for MgO and $MgAl_2O_4$ particles decreased with increased temperature and were almost identical (approximately 200 seconds for a 150 micron diameter particle at 1500 °C. This is physically sound since the MgO particles were covered by $MgAl_2O_4$. Al_2O_3 dissolution times were slightly longer (approximately 250 seconds for a 150 micron diameter particle at 1500 °C) than that of MgO and $MgAl_2O_4$ particles. No reaction layer was observed on the surface of the Al_2O_3 particles in the absence of MgO in the slag. Interestingly enough, pure $MgAl_2O_4$ was found to precipitate on Al_2O_3 particles in MgO containing tundish slags. **Table I** below summarizes the total dissolution times observed for the various cases.

Table I: Summary of the dissolution times observed for various inclusions.

Inclusion	Inclusion particle size	Slag	Temperature range	Typical dissolution time
Al_2O_3	110μm	Tundish	1470-1530 °C	225 seconds at 1500°C
Al_2O_3	110μm	Tundish (with 7.3% MgO)	1470-1530 °C	225 seconds at 1500°C
Al_2O_3	90 μm	Ladle slag	1470-1530 °C	60 seconds at 1500°C
Al_2O_3	150μm	36%CaO-21%Al_2O_3-42%SiO_2	1470-1550 °C	250 seconds at 1500°C
MgO	150μm	36%CaO-21%Al_2O_3-42%SiO_2	1470-1550 °C	200 seconds at 1500°C
$MgAl_2O_4$	150μm	36%CaO-21%Al_2O_3-42%SiO_2	1470-1550 °C	200 seconds at 1500°C
TiN	Irregular 50-100 μm	SiO_2-CaO-Al_2O_3-MgO	1300-1400°C	2-5 seconds

The reaction mechanisms were found to be either diffusion in the slag, reaction control at the interface or a mixture of the two. The diffusion coefficients in the liquid slag (and thus viscosity) and the thermodynamic solubility limits of the inclusions in the slags (providing the driving force for the dissolution reaction) were found to be the most pertinent slag properties for optimizing a slag with respect to inclusion dissolution.

The major impact of this work is the realization that slag design, from the point of view of inclusion dissolution rate, is as important as designing to ensure a controlled liquid flow field. This work also indicated that the dissolution rate of alumina is affected negatively by magnesia content in the slag and that high silica content slags, although they have a large capacity for alumina, have relatively slow dissolution rates. Both of these findings were quite novel and lead to a different view of ladle and tundish slag design for clean steel manufacture and pint out that a model of clean steel production must include, not only transport to the interface but the kinetics of interfacial separation

and particle dissolution. In this work dissolution rate is shown to be very important thus future models must include all of these steps.

This finding made the development of a model to predict the effect of processing time on clean steel formation not possible within the time constraints of this project; although, the key aspects of such a model are well developed. These findings also point out that such a model must include particle motion on many scales: globally in the liquid where the particles can grow and agglomerate, locally at the interface where the particle separate, and then globally as they dissolve in the slag. Clearly such a model must couple liquid steel flow to slag flow and would only have meaning as a model of an operating unit taking into account actual slag chemistries, volumes and reactions.

Objective 2: To develop a methodology to enable steels of less than 1 ppm total oxygen to be produced with an average inclusion diameter of less than 5 microns

In this work it was decided to study (1) the effects of temperature on potential oxygen levels, (2) reoxidation on steel cleanliness and (3) the potential for inclusion pushing by the solidifying interface as a mechanism for clean steel formation.

Temperature Effects

Removal of dissolved oxygen is one of the most important steps in steelmaking practice. This operation is principally carried out in the ladle by adding elements that have greater affinity to oxygen than iron such as aluminum, silicon, manganese, titanium, calcium etc. to the molten steel and finally by making a vacuum treatment of the melt. In fact, the elimination of oxygen consists almost in the reaction between deoxidizers and dissolved oxygen. This leads to a formation of solid inclusions that move to the interface metal/slag or remain in suspension in the molten steel. Total oxygen levels are used as a rough measure of steel cleanliness.

Although intensive work has been done on deoxidation of steel, some uncertainty still exists on the solubility limit of oxygen. Available thermodynamic data on deoxidation equilibrium of liquid iron are not necessarily in agreement with industrial results, because the influence of the interaction between different impurities has not been evaluated accurately enough.

The potential for clean steel, as measured by the total mass of oxide inclusions that can be formed in the liquid steel, is determined by thermodynamics of oxidation reactions, oxide solid inclusions stability, treatment temperature etc.

The deoxidation reaction is generally expressed as following:

$$x\,M + y\,O = M_xO_y \quad (1)$$

Its reaction constant is:

$$K = \frac{a_{M_xO_y}}{a_M^x \cdot a_o^y} \quad (2)$$

Were K and a_i represent the reaction constant and the activity of constituent i in the system respectively. a_i is related to the activity coefficient f_i, which is also linked to melt composition and interaction parameters.

$$a_i = f_i(\%i) \quad (3)$$

Where i represents M or dissolved oxygen in **Reaction (1).**

$$f_M = e_M^O \cdot (\%O) + e_M^M \cdot (\%M) \quad (4)$$

$$f_O = e_O^M \cdot (\%M) + e_O^O \cdot (\%O) \quad (5)$$

Where e_i^j represents the first order interaction parameter of j on i in the melt.

According to **Equation (2)**, total oxygen in steel is related to thermodynamic values that are involved in **Equations (2) to (5)**.

However, the equilibrium constant shifts in the direction to cause **Reaction (1)** to go to the right with falling temperature. Several research works were done to establish values of K as a function of temperature by assuming different values of activity coefficients as well as interaction parameters. Some values of K found in the literature [11, 12] are given in **Table II**.

More data on different deoxidizers are compiled in reference 10. However, no experimental data on oxygen solubility as function of temperature are available. Nonetheless, mathematical predictions of the direct relationship between dissolved oxygen and silicon [11] or manganese [12] and temperature were performed. **Figures 5 and 6**, calculated by Turkdogan, show a decrease in dissolved oxygen with decreasing temperature, for example.

Several investigators have assessed activity, activity coefficients and interaction coefficients by combining existing data and electrochemical measurements of oxygen partial pressure. Most of these data are for 1600 °C [10-12]. Only a few data are related to temperature, these are listed in **Table III**. The temperature dependence of these values makes a prediction of total oxygen at different temperatures possible.

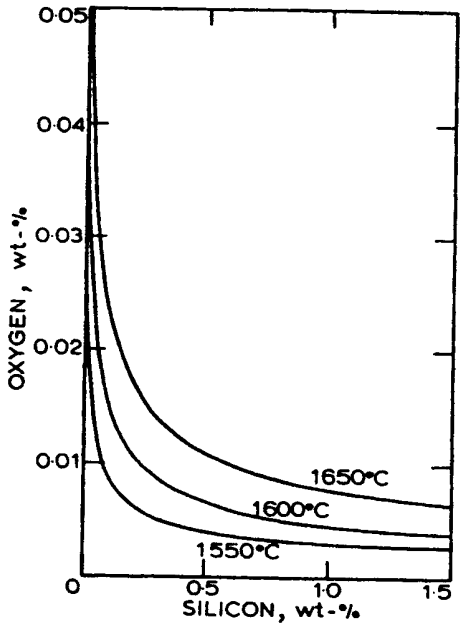

Figure 5: Oxygen solubility in Fe-Si melt as a function of Si content and temperature [11].

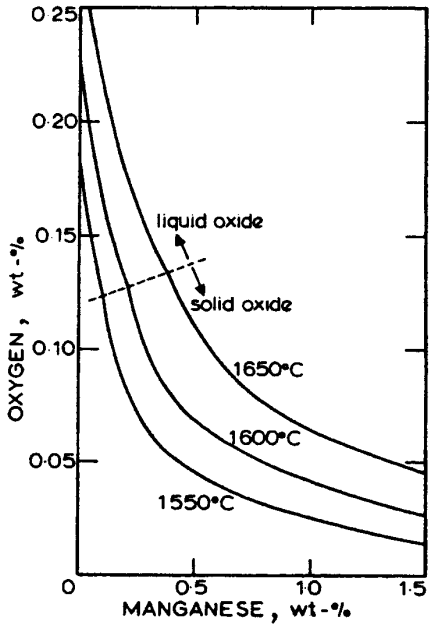

Figure 6: Oxygen solubility in Fe-Mn melt as a function of Mn content and temperature [12].

Previous research on deoxidation have lead to different values of residual dissolved oxygen in the steel as different deoxidizers were used [2]. However the results were related to the type and quantity of used deoxidizers and other parameters such as slag composition, oxygen partial pressure over the melt, temperature, etc. Lowest oxygen contents obtained that have been achieved at 1600 °C in previously published works are compiled in **Table V**. Even so, thermodynamic calculations show that it remains possible to reach very low oxygen contents in steel. For example when aluminum is used as deoxidizer, the equilibrium level of soluble oxygen in liquid steel is around 10 ppm at 1600 °C with soluble aluminum of 0.05 wt. %. When aluminum killed steel is treated with calcium, decreasing the alumina activity in slag, it is thermodynamically possible to reach less than 1 ppm of dissolved oxygen in steel. Thus the potential for steel cleanliness in aluminum deoxidation is less than 1 ppm [1]. This can also be much lower when the treatment temperature decreases.

Table II: Deoxidation constants of some deoxidation reactions.

Reaction	[M]	Log K
$FeAl_2O_4$ = 2 Al + 4 O + Fe	< 1 ppm	-71600/T + 23.8
Al_2O_3 = 2 Al + 3 O	> 1 ppm	-62780/T + 20.1
CO = C + O	> 0.02 %	-1168/T - 2.07
MnO = Mn + O	> 1%	-14450/T + 6.43
SiO_2 = Si + 2 O	> 20 ppm	-30410/T + 11.59

Table III: First order interaction coefficients as a function of temperature in liquid iron.

j → ***i***	**Al**		**Si**	**C**		**O**	
Al	63/T + 0.011	80.5/T		380/T – 0.023	158/T + 0.058	-34740/T + 11.95	-17667/T + 7.58
C			162/T – 0.008	----	0.184		
O	-20600/T + 7.15	-10477/T + 4.50			0.1	-1750/T + 0.734	-1750/T + 0.76
Ref.	11	10	11	11	10	11	10

Table IV gives different interaction parameters at different temperatures of deoxidation reactions.

Table IV: Interaction parameters of deoxidation [2, 15].

M ?	T (K)	Log K_M	$e_O^{(M)}$	$e_M^{(O)}$	$e_M^{(M)}$	$e_O^{(O)}$	$r_M^{(O)}$	$r_O^{(M)}$	$r_O^{(M,O)}$	$r_M^{(O,M)}$
Mg	1823	-6.87	-305	-464	---	-0.200	412,000	-22,500	544,000	-68,500
	1873	-6.80	-280	-426	---	-0.174	350,000	-20,000	462,000	-61,000
	1923	-6.73	-257	-390	---	-0.150	292,000	-17,700	385,000	-53,800
	1948	-6.70	-245	-373	---	-0.138	263,000	-16,600	348,000	-50,400
	2023	-6.61	-213	-323	---	-0.105	183,000	-13,300	242,000	-40,600
Ca	1823	-7.25	-336	-835	---	-0.200	739,000	-19,500	591,000	-98,000
	1873	-7.15	-310	-771	-0.002	-0.174	650,000	-18,000	520,000	-90,000
	1923	-7.05	-286	-710	---	-0.150	566,000	-16,600	453,000	-83,000
	1948	-7.00	-274	-680	---	-0.138	525,000	-15,900	420,000	-78,000
	2023	-6.86	-241	-596	---	-0.105	409,000	-14,000	327,000	-70,000
Al	1823	-13.23	-1.25	-2.12	0.044	-0.200	44	-0.010	52	-0.0134
	1873	-12.57	-1.17	-1.98	0.043	-0.174	40	-0.010	47	-0.0136
	1923	-11.94	-1.09	-1.84	0.042	-0.150	36	-0.010	43	-0.0138
	1948	-11.63	-1.05	-1.78	0.041	-0.138	34	-0.010	41	-0.0139
	2023	-10.77	-0.94	-1.59	0.040	-0.105	29	-0.009	34	-0.0142

According to values given in **Table V**, the lowest oxygen content that was ever reached at 1600 °C is 2 ppm. This result was obtained by Dimitrov et al. [3] who used aluminum as deoxidizer in laboratory scale. The oxygen content could be very low if other strong deoxidizers like zirconium or other rare earth elements were used. Calculations made by Janke and Fischer [4] using existing thermodynamic data give 0.2 ppm dissolved oxygen in liquid steel when zirconium is used as deoxidizer. Unfortunately, these potential

deoxidizers are significantly more expensive than aluminum, silicon and manganese. Therefore, their use could be confined to specific cases, where specific oxygen content or solid inclusions in steel must be very low.

Table V: Oxygen contents in steel melts at 1600 °C.

Deoxidizing	Al	Mg	Ca	Ti*	Zr*	Al-Mg
Temperature [C]	1600	1600	1600	1600	1600	1600
[O] ppm	2	3.4	1.9	1.6	0.2	3.5
[M] ppm	3000	18	18.1	24000	6000	4910-26.5
Ref.	3, 9	2	2	8	8	2

* calculated.

In general, earlier research works show that steel deoxidation is related to, among other parameters, the content of the deoxidizer and oxygen partial pressure over the melt. But it is clear that the total oxygen content as a function of deoxidizer content is still controversial. Previous published data do not show a continuous decrease in oxygen content but, in the contrast to this, a parabolic curve with a minimum and then a pickup in oxygen when the total oxygen content is plotted versus the deoxidizer content. **Figure 7** is an example of experimental results of deoxidation with aluminum obtained by several authors. According to previous publications, this could be explained by the fact that the solubility of oxygen is higher in pure deoxidizers than in iron and also by changes in the activity coefficients of oxygen and deoxidizers expressed in **Equations (4) and (5)** [11, 12]. However, the net oxygen leveling steel depends on the extent of its pickup and removal during various stages of steelmaking and casting.

In addition, deoxidation reaction products are usually solid inclusions that remain floating on the top of the melt or in suspension. This is also a fraction of the steel total oxygen. Consequently, the elimination of oxide solid inclusions will contribute to reduce the total oxygen of the melt. Successful investigations on the behavior and the removal of oxide solid inclusions from steel melts have been done [1, 5-8].

The solubility of oxygen in iron decreases with decreasing temperature, thus refining must be carried out at temperatures lower than 1600 °C. The stronger the deoxidizer, the more pronounced is the temperature effect. It is well known that deoxidation reactions are exothermic; consequently reactions are more quantitative with decreasing temperature. Thus there are three issues in producing clean steels: (i) avoiding reoxidation, (ii) reducing processing temperatures, and (iii) removing inclusions once formed or preventing inclusions from being entrapped in the growing steel shell.

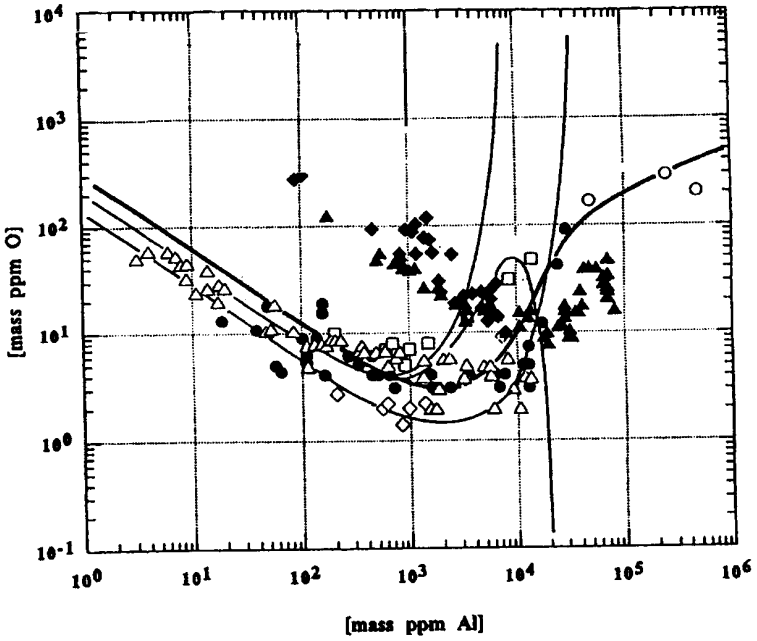

Figure 7: Oxygen vs. aluminum content in iron melts at 1600 °C [2].

Total oxygen contents of solid samples are usually measured by vacuum-fusion analysis, neutron-activation or inert-gas fusion-infrared absorptiometry technique [12, 13, 14]. The determination of oxygen in iron alloys is more accurate by using the inert-gas fusion-infrared absorptiometry than with the other techniques [14]. Meanwhile, both techniques are used for oxygen contents greater than 5 ppm. Oxygen levels in iron as low as theoretically predicted cannot be measured experimentally or achieved using these techniques. However, in the industrial practice the oxygen content of iron is generally assessed from oxygen partial pressure measured by means of an oxygen sensor. Using this method, knowledge of accurate values of activity, activity coefficients and interaction parameters of the components involved in the system is necessary. Up to date existing techniques are not precise enough to measure very low oxygen contents (1 ppm or less). Nevertheless, a mass balance could be used to assess the oxygen content when thermodynamic data, i.e. activity and/or activity coefficients of the components involved in the system are fairly established. This will also necessitate a precise sample chemical analysis that should differentiate dissolved metals and metals in form of oxides. Once accurate values of activity or activity coefficient as well as precise chemical analysis are available, a numerical model for predicting total oxygen concentration during deoxidation can be developed from experimental results.

A number of experiments were conducted to determine if liquid iron could be significantly under-cooled to allow processing at temperature significantly below the liquidus.

The sessile drop technique was used. A brief summary of the apparatus is given below. A horizontal resistance furnace with a $MoSi_2$ heater was used and an Al_2O_3 reaction tube (3 inches in diameter and 42 inches in length) was placed in horizontal position and sealed with two water jackets at the ends of the tube. A Pt-Rh6%/Pt-Rh30% thermocouples was placed on the tube to control the temperature. Argon was purified by flowing the gas over heated copper, magnesium and titanium. An oxygen sensor was used to measure the oxygen partial pressure in the argon gas, and measured the oxygen partial pressure of the exhaust gas from the reaction tube. To eliminate issues of magnesium oxide substrate purity, single crystal magnesium oxide substrate materials were purchased from Alfa Aesar. The surface of the magnesium oxide substrate is (100) plane, and the surface roughness, Ra, of the single crystal was measured as 0.02 micron. The iron samples were also purchased from Alfa Aesar and were of the following chemistry: 99.9985% Fe, which included measurable impurity contents of Cu 1 ppm, Mg 2 ppm and Ti 2 ppm. The weight of the sample was always set to 2.5 g.

A recalescence of the iron drop on the oxide substrate, which indicates the onset of solidification, was observed in an argon gas atmosphere when the temperature was decreasing. The results are summarized in **Figure 8**. The shape of the sample on the magnesium substrate changed as shown in **Figure 9**, just after the recalescence of the sample was observed. This shape change was observed 3 times with the oxygen partial pressure $1x10^{-18}$atm. The recalescence of the iron drop on the magnesium single crystal substrate is shown in **Figure 10** with an elapsed time. The recalescence was observed within 1 frame of video image, 1/30 s. Then, the temperature of the iron drop decreased rapidly and came back to the substrate temperature within 5 s. The undercooling was also measured as a function of oxygen partial pressure in the range from 10^{-19} to 10^{-17} atm as shown in **Figure 8**. The undercooling is increasing with increasing oxygen partial pressure.

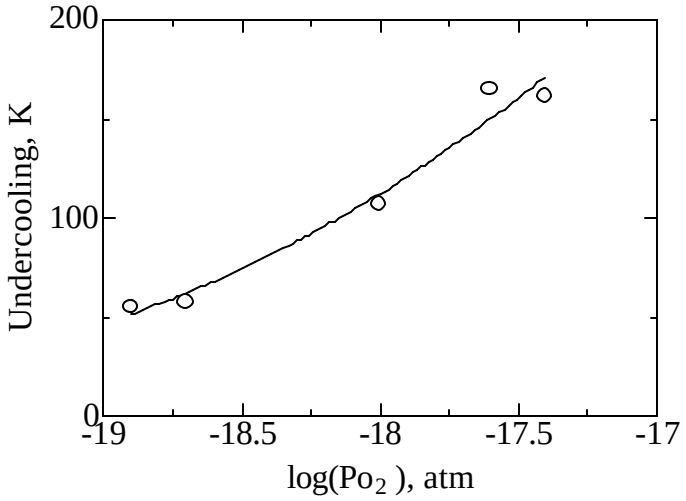

Figure 8: Undercooling as a Function of Oxygen Partial Pressure.

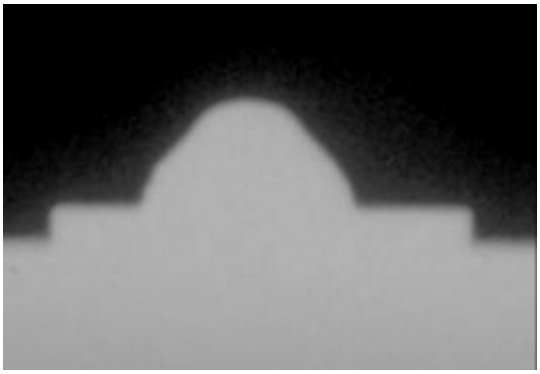

Figure 9: Droplet Shape Change Due to Solidification.

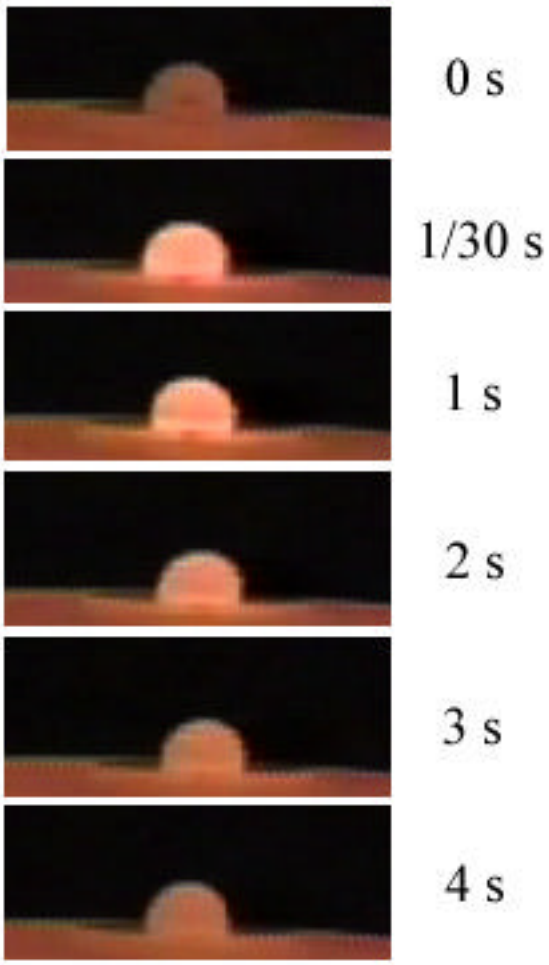

Figure 10: Droplet Recalescence at 200 K undercooling.

Thus it is in fact possible to deeply undercool liquid iron alloys by controlling oxygen partial pressure in the gas atmosphere. This leads to the potential for a new way to produce clean steels – equilibrate with low oxygen partial pressure inert gases at temperatures below the liquidus. The potential for very low oxygen contents by this process is remarkable as oxygen activities significantly below 1 ppm are possible. As very low oxygen contents are possible, under conditions where liquid steel will solidify very quickly (as shown in **Figure 10**), inclusion size distribution will be very small, smaller than current processes. Thus this technique has the potential to produce steels with oxygen levels below 1 ppm with inclusions with an average inclusion diameter of less than 5 microns.

Reoxidation of Steels

The re-oxidation process involves: (i) transport of oxygen to the melt, (ii) mass transport in the melt, (iii) precipitation of the oxide phase (iv) growth of the oxide precipitate and (v) agglomeration into a macro-inclusion.

Gas phase mass transfer to a melt has been extensively studied and documented in the literature and models based on experimental results have been used to predict the melt re-oxidation rates in the tundish based on gas phase mass transfer through the tundish inlet and top covering tundish powder. Precipitation of the oxide phase follows a chemical reaction between metallic elements in the melt (unreacted de-oxidation reactants such as Al, Si or Ca and/or Fe) and oxygen dissolved in the melt and the thermodynamic basis of this reaction is essentially similar to the well studied de-oxidation equilibrium that takes place in the ladle. It should however be mentioned that unlike de-oxidation that occurs under isothermal conditions (at $\approx 1600^{o}C$) where thermo dynamic data are abundant, re-oxidation occurs more often under significantly lower and often changing temperatures where published interaction coefficient data are more scarce.

The evolution of the oxide precipitates in steel melts, in terms of size and shape, is an important issue since oxide size is well known to be an important factor in the mechanical properties of the final steel products were large macro-inclusions are known to be especially detrimental. On the other hand, inclusion removal by flotation through the bath, following Stokes' law, is favored when the inclusion size is large. It is therefore important to be able to predict the inclusion size evolution with time. Oxide size evolution occurs generally by one or both of two mechanisms, crystal growth and/or agglomeration. In the case of crystal growth of Al_2O_3 in steel melts, a recent study indicates that high super-saturation leads to the formation of spherical particles or when impurity adsorption took place plate-like particles. Non-uniform super-saturation over the particle surface leads to dendrite formation. Under low super-saturation, near equilibrium, conditions, the particles were found to become facetted. When simultaneous growth and sintering occurred, the particles assumed octahedral forms.

Agglomeration and sintering, is driven by surface tension reduction and is highly favored in the case of Al_2O_3 in steel due to non-wetting conditions. Particle agglomeration is accelerated by particle collisions in the melt. In addition, when a gas phase is present at free surfaces or gas bubbles, clustering can occur for solid Al_2O_3 through attractive forces caused by capillary depression of the melt meniscus.

While the inclusion types resulting from different super-saturation conditions has been documented there is little data on the actual kinetic rates of crystal growth due to the experimental difficulties that occur in accurately measuring alumina growth rate at high temperatures under oxidizing conditions. (CSLM) equipped with a gold image furnace. In this work *in-situ* observations through a CSLM combined with SEM-EDS is used to quantify the growth of Al_2O_3 at steel/gas interfaces due re-oxidation. The effects of gas flow rate, low and high oxygen partial pressure and temperature were investigated and the results discussed in terms of thermodynamics and kinetics.

The experimental approach undertaken in this study was to observe the re-oxidation process on the surface of the molten steel samples, using a high temperature Confocal Scanning Laser Microscope (CSLM) under controlled temperatures, flow rate and atmosphere, and analyze the inclusions after the experiments with a scanning electron microscope (SEM) combined with energy dispersive spectrometer (EDS).

The CSLM utilizes confocal optics and a laser light source, and when equipped with a gold image high temperature furnace, it is capable of real time 3D imaging of uneven surfaces such as a high temperature liquid-gas interface. The high speed scanning by the acousto-optical device (AOD) enables confocal images to be obtained at a rate of several hundred times faster than with the standard confocal microscope. With this system, it is possible to collect a series of images of in focus layers and combine them into a single three-dimensional image in real time. Therefore, the CSLM is ideally suited for *in-situ* study of fluid flow, chemical reaction and phase transformation.

A high temperature gold image furnace was used to melt samples by reflecting the light of a halogen bulb on the sample. The steel samples were placed in cylindrical Al_2O_3 crucibles of 5.5 mm diameter and 3 mm height which were put in a Pt/Al_2O_3 sample holder. The sample holder is equipped with a B-type thermocouple which is used to monitor the approximate temperature in the hot zone. Actual temperature of the sample was estimated by calibrating the thermocouple reading with the melting points of pure Ni, Ni and Cu. The atmosphere inside the gold image furnace was controlled by monitoring the oxygen partial pressure in the outgoing gas with a solid state stabilized ZrO_2 based oxygen probe.

Upon melting, irregular inclusions of sizes similar to the original de-oxidation inclusions were found to float up to the surface. They were not seen to grow and would move to the crucible edge and disappear after a while likely due to the surface fluid flow and curved shape of the molten steel meniscus. These inclusions are likely not a result of re-oxidation but assumed to be the existing de-oxidation inclusions. The melt surface was, after the disappearance of these initial inclusions clean. After a length of time or after the pulse of Ar-air gas, re-oxidation occurred and the inclusions either grew dendritically or formed aggregates due to collision and sintering. The nature of this re-oxidation process in terms of the time delay until it was observed, growth and agglomeration rates, inclusion chemistry and the effects of atmosphere, gas flow rate and atmosphere were the focus of this investigation.

The re-oxidation process was significantly different when Ar gas was used compared to when an air/Ar mixture was used. In the absence of air the re-oxidation occurred first at the crucible center with a few individual inclusions growing and clustering as shown in **Figure 11**. These inclusions would subsequently move towards the container wall and from there continue to grow dendritically towards the center on the melt surface as show in **Figure 12**.

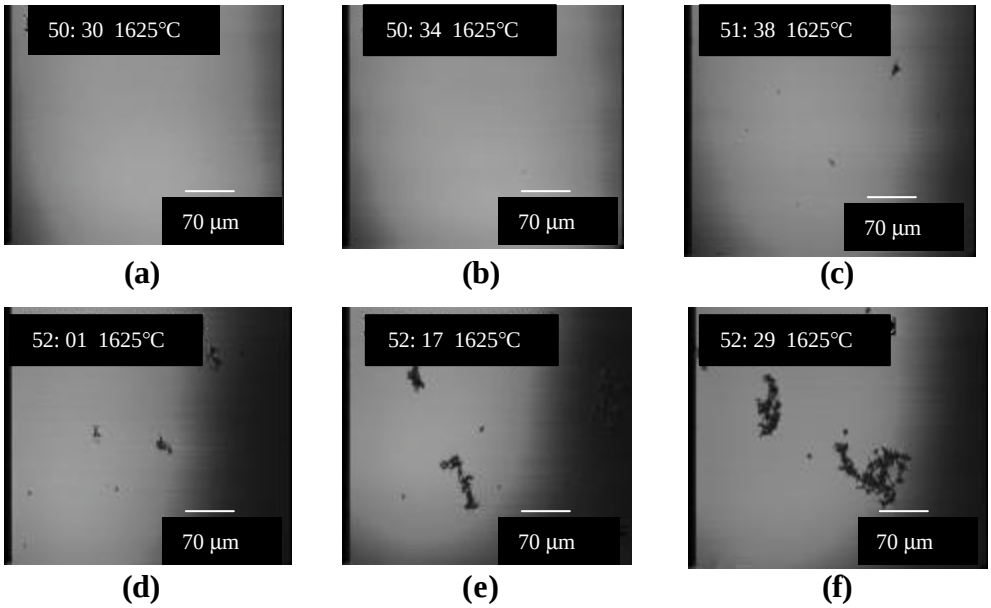

Figure 11: Oxides formation, growth and agglomeration due to the re-oxidation.

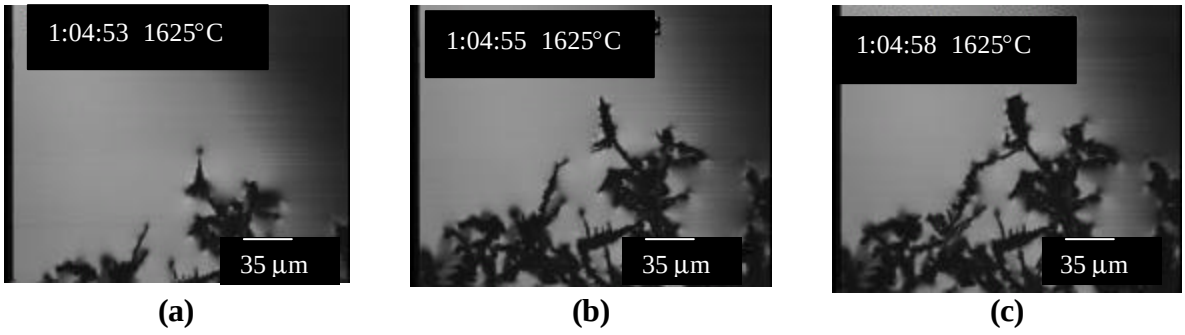

Figure 12: Dendritic phase growth from the crucible/melt interface towards the center.

When air/Ar mixture was used, individual inclusion formation was observed uniformly on the surface as shown in **Figure 13**. These inclusions would initially grow and after reaching a certain size cluster and agglomerate, resulting in an open network covering the melt surface.

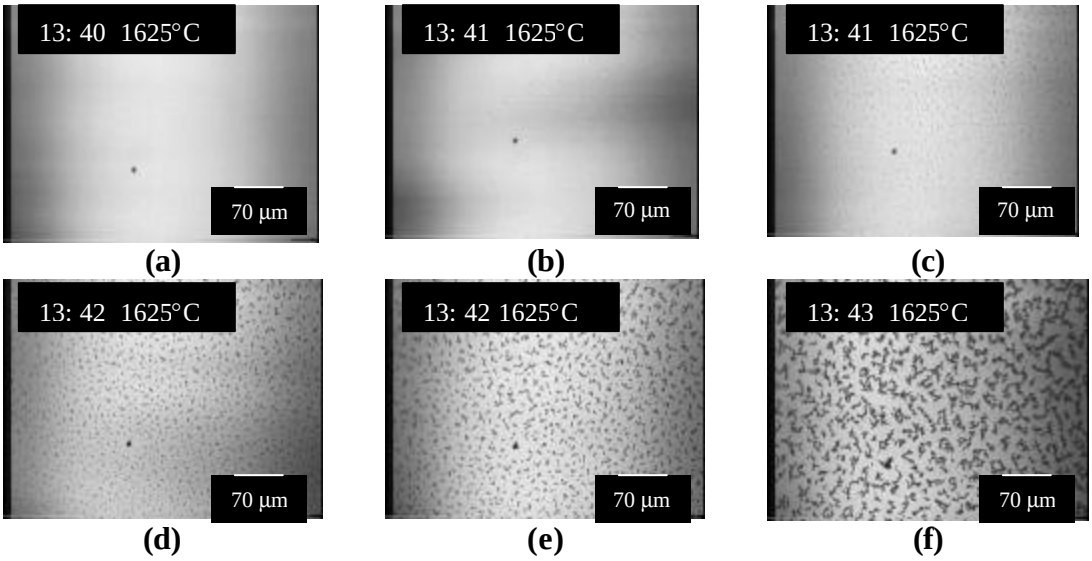

Figure 13: Inclusion formation, growth and agglomeration during re-oxidation under air/Ar mixture.

SEM-EDS analysis results, shown in **Figures 14 and 15**, of the inclusions after the high temperature experiments showed that in the cases when Ar was used, the inclusions were pure Al_2O_3 and in the cases were air/Ar was used the inclusions contained Fe/Al at a ratio similar to that of hercynite ($FeAl_2O_4$).

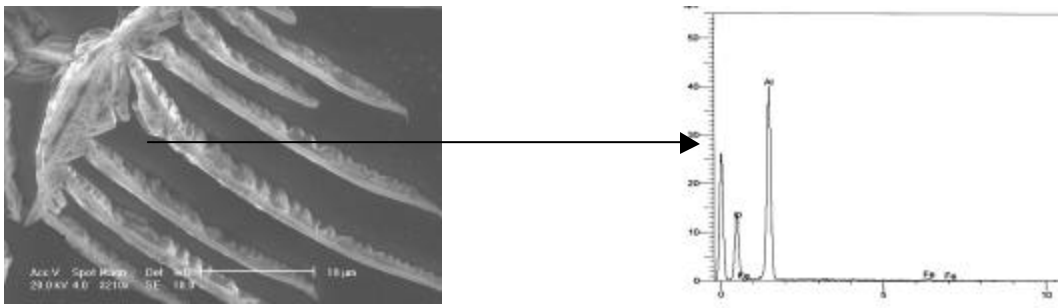

Figure 14: The SEM-EDS results of inclusions resulting from re-oxidation in an Ar atmosphere.

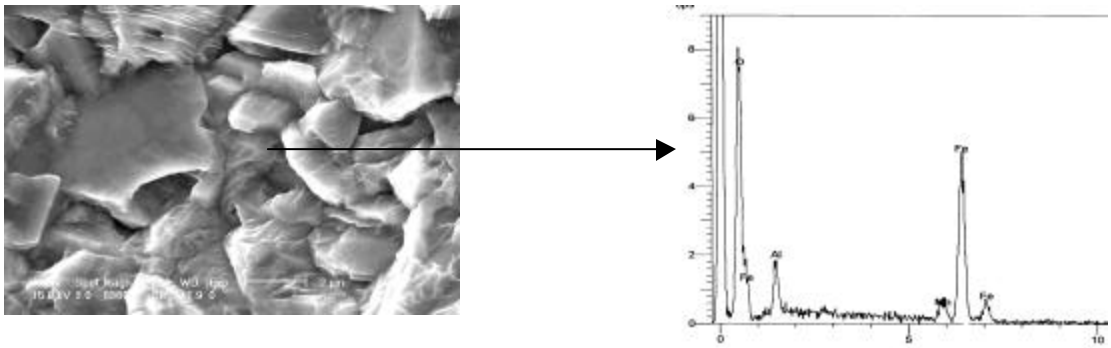

SEM EDS

Figure 15: The SEM-EDS results of inclusions resulting from re-oxidation in an air/Ar atmosphere.

In summary, it was found that:

1. Under low oxygen pressure conditions, re-oxidation produced Al_2O_3 first at the crucible center with subsequent oxide growth and inclusion agglomeration. Afterwards these clusters moved towards the container wall from where they continued to grow dendritically. When air/Ar was used, $FeAl_2O_4$ formation was observed uniformly on the melt surface, and the inclusion agglomeration resulted in an open network.
2. Re-oxidation did not cause immediate formation of observable oxides and there was a significant time delay between introduction of oxygen and observation of an oxide. This suggests that the surface of the liquid steel was supersaturated with respect to oxygen before the inclusions formed and grew.
3. The time period necessary for the observable re-oxidation to occur is a function of isothermal temperature and flow rate. At higher temperatures, it took longer for the dissolved oxygen to reach the super-saturation at which re-oxidation would occur. This time period was also different at different gas flow rates, which suggests a gas phase mass transfer mechanism of oxygen in the atmosphere through a gas boundary layer to the melt surface controls super-saturation and subsequent inclusion formation.
4. The oxides resulting from re-oxidation grow and agglomerate after formation. The growth rate was controlled by the diffusion of the solvent towards the particle surface. The attraction force between the adjacent inclusion pair during agglomeration was found to be over 10^{-17} N.

These experiments suggest that reoxidation can be a significant issue as it appears that a significant supersaturation is necessary to precipitate an alumina inclusion. Thus, variation in the measurements of steel cleanliness may be simply a result of reoxidation at levels that were not high enough to result in inclusion precipitation. This would lead to significantly higher measurements of total oxygen than the equilibrium value. Thus in

any clean steel operation with a goal of less than 1 ppm total oxygen, elimination of reoxidation will be a major issue which must be overcome.

Inclusion Pushing by the Solidification Interface

CSLM combines the advantages of confocal optics and a He-Ne laser and makes it, thereby, possible to observe samples at high resolution at elevated temperatures. The confocal optics enables the (i) detection of a strong signal from the focal plane while (ii) decreasing the intensity of signals not in the focal plane. By scanning a surface at various focal depths, a 3-dimentional image is constructed and thus images of uneven samples with depths and pimples can be obtained. The utilization of a laser results in high illumination intensity compared to the thermal radiation at elevated temperatures and thus increases the resolution between different phases. This technique is ideally suited for *in situ* study of fluid flow, chemical reaction and phase transformation involving molten metals, fluxes and refractory linings and is therefore being employed at the Center for Iron and Steelmaking Research at Carnegie Mellon University for investigating high temperature metallurgical phenomena.

In the current research the steel samples were placed in cylindrical Al_2O_3 crucibles of approximately 5 mm diameter and 3 mm height and heated inside the CSLM hot stage under an ultra pure Ar gas purified by dryerite and heated Cu and Mg chips. The oxygen potential thus established was 10^{-16} atm. After melting the samples, the temperature was lowered in order to allow for solidification. The observations of the advancing front were made from the top as the front grew from the walls towards the center of the crucible. Observed images were exported to a video recorder and the inclusion size and solidification rate were analyzed with an image analysis software.

The steel samples were Al-killed low-carbon steels. The dissolved oxygen in this grade is generally at 2×10^{-4} wt%. The natural inclusions found in this sample were verified through Scanning electron microscope (SEM) combined with Energy dispersive spectrometer (EDS) to be globular Al_2O_3-CaO-MgO inclusions and in some cases irregularly shaped Al_2O_3 inclusions.

The focus of this study was placed on the following three fundamental phenomena at the solidification front: (i) The pushing/engulfment of solid Al_2O_3 inclusions (ii) the pushing/engulfment of liquid Al_2O_3-CaO-MgO inclusions and (iii) the entrapment of inclusions at the intercellular regions. The comparison between the measured results and predictions for Al_2O_3 inclusions is shown in **Figure 16**.

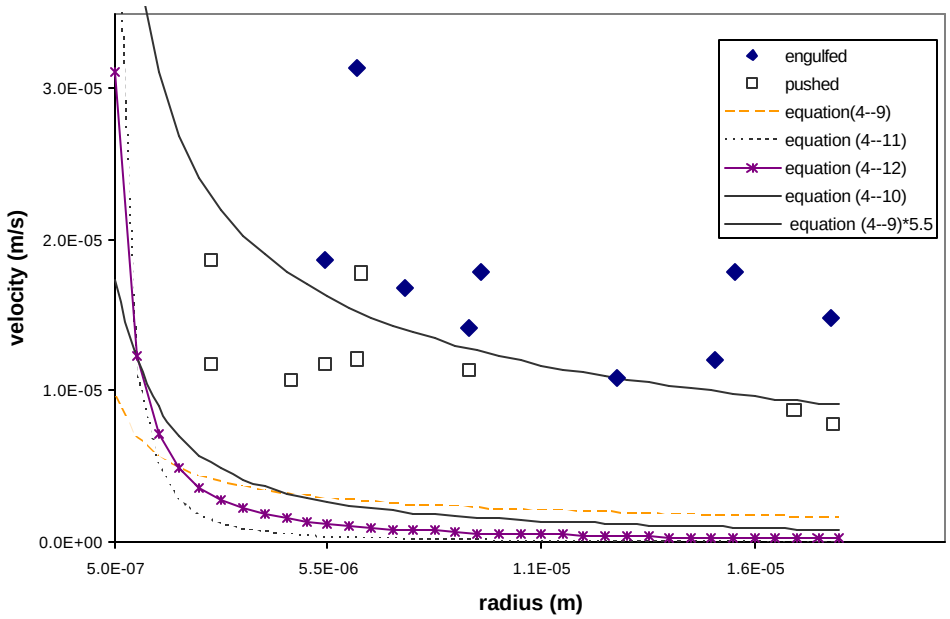

Figure 16: Comparison between measurements and predictions of pushing *vs.* engulfment of solid Al_2O_3 inclusions.

It can be seen that all four predictive models (**Table VI**) underestimate the critical velocity significantly; however reasonable agreement can be found for liquid slag inclusions. For entrapment versus escape at the cellular grain boundaries (with dihedral angle of 25°) it was found that inclusions slid along the front into the boundary at low solidification velocities and liquid inclusions were more readily engulfed while no appreciable difference was observed for the large solid inclusion clusters.

The major finding of this study is that one can predict the solidification velocity at which particles would be pushed rather than gathered and this indicates another method of producing ultra clean steels where the casting apparatus would be design to allow the solidification front to grow at a rate that would push inclusions ahead of it. Thus the inclusion could be pushed to a given volume in the casting, which could then be removed. In this manner all precipitated inclusion could be removed.

Table VI: Particle pushing/engulfment models in literature.

Equation	Ref.	Comments
$v_{Cr} = \left(\frac{\Delta g_0 \cdot a_0^2}{3hK \cdot r} \right)^{1/2}$ (6)	Stefanescu *et al.*	v_{Cr} given by apex of v_{eq} *vs. d*
$v_{Cr} = \frac{1.3\Delta s}{h} \left(16 \left(\frac{r}{a_0} \right)^2 K(15K + x) + x^2 \right)^{-1/2}$ (7) $\Delta s = s_{PS} - s_{PL} - s_{SL}$ $x = \frac{c_\infty \lvert m_L \rvert \Delta s}{K_C G h D}$	Pötschke and Rogge	Critical velocity occurs when viscous and interfacial forces are equal. Accounts empirically for impurities
$v_{Cr} = \frac{n+1}{2} \left(\frac{\Delta H \cdot a_0 \Omega D_L}{k_B T r^2} \right)$ (8) $4<n<5$	Uhlmann *et al.*	Critical velocity occurs when *d* becomes unstable and the chemical potential decreases with decreasing *d*.
$v_{Cr} = \frac{0.14 \cdot B^{2/3} s_{SM}^{1/3}}{h r^{4/3}}$ (9) $B=10^{-21}$ J	Chernov *et al.*	-
Required fluid velocity for particle escape: $v_L \geq r \left(\frac{2A}{9h} (r_P - r_L) g + \frac{A}{h} \frac{v_s}{r} \right) \frac{f + \tan q}{1 - f \cdot \tan q}$ (10)	Han and Hunt	Force balance in vertical direction gives the critical velocity for particle escape through sliding

$C_¥$ = concentration of the second, dissolved component in the melt, m_L = the gradient of the phase diagram liquidus line, K_C =distribution coefficient, G = the undisturbed temperature gradient, D = the diffusion coefficient of the impurity in the melt, DH = latent heat of fusion per unit volume, D_L = the diffusion coefficient for matrix liquid, W = atomic volume, k_B = Boltzman's constant, T = temperature, A =constant, f = coefficient of friction, q = roughness parameter, v_S = the growth velocity of the macroscopic solid-liquid interface.

<u>Objective 3</u>: To determine the slag-metal interface conditions necessary for ultra clean steels

Slags and their properties play a crucial role in the removal of non-metallic inclusions during clean steel manufacturing. Non-metallic inclusions are generally removed in the ladle, tundish and continuous casting mold. In all of these vessels, the molten metal is covered by a molten slag in order to provide thermal and chemical protection and in the case of the caster to also lubricate the mold/strand interface. Inclusions are removed by (i) transporting the inclusion to the steel/slag interface, (ii) separating across the interface and (iii) dissolving into the slag phase.

Among the three steps for inclusion removal, the second step involving separation across the interface is probably the least understood and is strongly influenced by interfacial properties. The thermodynamics of inclusion removal has been studied in a number of papers [18-22]. Consider an inclusion at the slag/metal interface. For an inclusion to be removed it is necessary for it to travel through the slag/metal interface and on into the slag phase. In terms of interfacial energies, a favorable separation will be achieved, from a thermodynamic view point, when the free energy change of **Equation (11)**, is negative:

$$\Delta G = g_{inclusion/slag} - g_{inclusion/metal} - g_{metal/slag} \qquad (11)$$

While the above mentioned model for separation of inclusions across a metal/slag interface is based on thermodynamics it is rather simplified and thus its applicability limited since the kinetics may be slow. As a spherical particle approaches the interface, the film between the particle and the other phase has to be drained and the hydrodynamic forces will determine the speed. At closer distances to the interface, the assumption of a continuous medium is no longer valid and the thin liquid film ahead of the particle will be removed slower. The final rupture of the interface is probably rapid as this has been found in the case of droplet separation. The residence time of particles at a fluid/fluid interface may thus be long although it is energetically favorable to separate it from one phase to another. The steps of drainage and rupture are schematically shown in **Figure 17**.

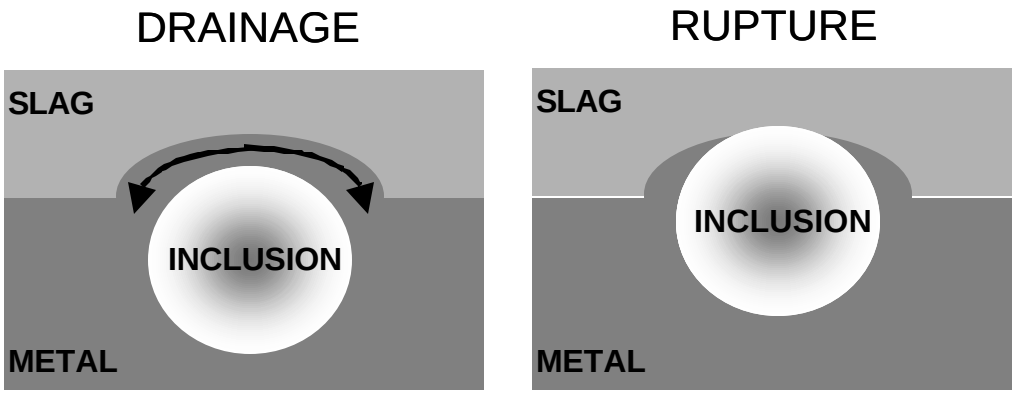

Figure 17: Schematics of kinetic/transport issues in inclusion separation across metal/slag interfaces.

The separation time would likely depend strongly on whether the inclusion is solid or liquid. In the case of solid inclusions, it is primarily a hydrodynamic problem. Bouris and Bergeles [23] and Nakajima and Okamura [24] and Cleaver and Yates [25] have all studied the mechanism of solid particle separation across steel/slag interfaces. Firstly, the existence of a film (that needs to be drained) was contingent upon the Reynolds number, i.e. if Re < 1, no film formation was assumed. The drainage step was computed based on a (i) force balance between the buoyancy on one hand and the drag, gravity and a so called *rebound force* on the other and (ii) fluid flow pas a sphere. The rebound force resulting from a normal interfacial stress is a function of the steel-melt/slag interfacial tension ($\sigma_{melt/slag}$). It should be mentioned that the presence of Marangoni forces might delay the drainage due to differences along the droplet surface as explained for the case of drainage around gas bubbles. Upon reaching a critical separation from the interface, the interface was assumed to be rupture and continued separation occurred based on the balance between the drag, buoyancy and the dynamically changing interfacial forces. Here, as long as the inclusions were not wetted by the melt, i.e. $\sigma_{inclusion/melt} > \sigma_{inclusion/slag}$, the inclusions would initially be pushed towards the slag. According to Bouris and Bergeles' calculations, an Al_2O_3 inclusion of 20 μm, would separate completely into a SiO_2-Al_2O_3-CaF_2-MgO-CaO (mould flux type) slag within roughly 0.5×10^{-5} seconds. Thus separation of solid inclusions at an interface is not a major issue as long as they can then be completely dissolved in the slag. Thus for clean steel formation in solid inclusion based steels, inclusion dissolution is the major issue in clean steel formation.

The separation of liquid inclusions was investigated at Carnegie Mellon by monitoring the molten slag metal interface through a transparent 50 wt.%CaO-50 wt.%Al_2O_3 slag with the CSLM. The steel sample was a low carbon Mn and Si killed steel. Two types of inclusions were predominantly found in the steel samples when characterized by SEM-EDS; globular MnO-SiO_2-Al_2O_3 that is liquid in molten steel and solid irregular Al_2O_3 inclusion clusters. The liquid inclusions could be seen to separate across the interface by gradually emerging from the steel meniscus within 1-2 seconds (**Figure 18**). Upon

emergence, the inclusions disappear from sight, presumable by being incorporated into the transparent slag. On the other hand, separation of the solid inclusions could not be observed and they were present on the metal side of the interface. They did not dissolve in the slag due to the fact that the slag/metal sample was being contained in an Al_2O_3 pan which saturated the slag with respect to Al_2O_3.

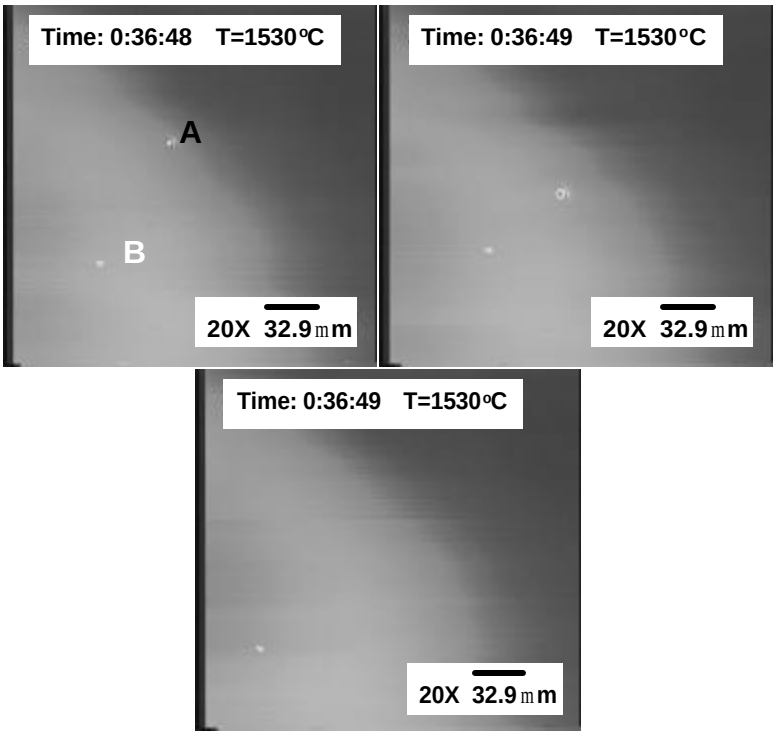

Figure 18: A liquid inclusion A emerges from the steel melt and disappears upon separation by dissolving into the transparent slag. Inclusion B is a solid Al_2O_3 inclusion.

The fact that the solid inclusion separation could not be observed suggests a rapid process which is in agreement with the fast separation times computed by Bouris and Bergeles (although the slag systems are markedly different). It is hard to explain the longer separation time of the liquid inclusions. The appearance of a gradual emergence in **Figure 18** suggests that the expansion of the ruptured interface is taking place but since the liquid $MnO\text{-}SiO_2\text{-}Al_2O_3$ inclusions are soluble in the slag the existence of a slag/inclusion interface is unlikely. Therefore the film drainage is likely the rate limiting factor and the appearance of a gradual emergence might be caused by a deformation in the steel/slag interface.

The drainage at a liquid inclusion is however more complicated by the fact that the inclusion is deformable and thus a dynamic shape change has to be accounted for continuously during the drainage. This would likely be affected by electrostatic and van der Waals forces and possibly polymeric anions in the slag or inclusion at the interface

and the viscosities of the film, slag phase and inclusion. To the best of the author's knowledge the film drainage at the slag/steel/liquid inclusion system has not been modelled. It is however likely that interfacial forces and film viscosity will play a key role similar to the drainage around gas bubbles during foaming.

Most liquid inclusions that separate at slag-metal interfaces are either liquid deoxidation inclusions or emulsified slags. It was therefore decided to observe the separation of liquid calcium aluminate inclusions at a gas-metal interface.

Upon melting the steel sample, liquid globular Al_2O_3-CaO-MgO inclusions could be observed on the melt surface. It is hard to establish the exact composition of the inclusions since they fall within a compositional range in the starting solid steel samples. If the small MgO content is neglected, the inclusions, upon melting of the steel matrix, would form various phases or phase mixtures depending on their starting compositions. These liquid or semi-liquid inclusions did not agglomerate with each other, even at very small separation distances. This indicates that attractive forces did not operate between these inclusions. In the case of liquid inclusions, the melt surface in between the particle pair is not appreciably depressed compared with the outer surface, and therefore, capillary forces do not operate between liquid particle pairs.

As the melt was solidified, inclusions were pushed or engulfed by the advancing front depending on their sizes and the advancing rate of *d* phase. A detailed study of the pushing *vs*. engulfment phenomena was carried out in an earlier study, and it was found that beyond a critical solidification velocity of the *d*-ferrite the inclusions would get engulfed. SEM-EDS analysis of the engulfed inclusions found at the interior of the samples was Al_2O_3-CaO of various compositions but free of any S. On the other hand the pushed inclusions evolved to become larger and irregular as solidification proceeded.

An example of the observed change in the inclusion size and shape at 1510°C is shown in **Figure 19**. When analyzing these inclusions after the experiments in SEM-EDS, they were found to contain appreciable amounts of S. A typical chemical map of such an inclusion is shown in **Figure 20**. **Figure 20a** shows a SEM picture about an inclusion core surrounded by a ring. The chemical composition in the core is enriched in Al and O, while the ring is mostly composed of Ca and S. The CaS shell was observed to be non-porous even at the magnification of ×500000. Thus during cooling these inclusion change from liquid to solid and completely change their character.

Figure 19: Inclusion change due to precipitation of CaS.

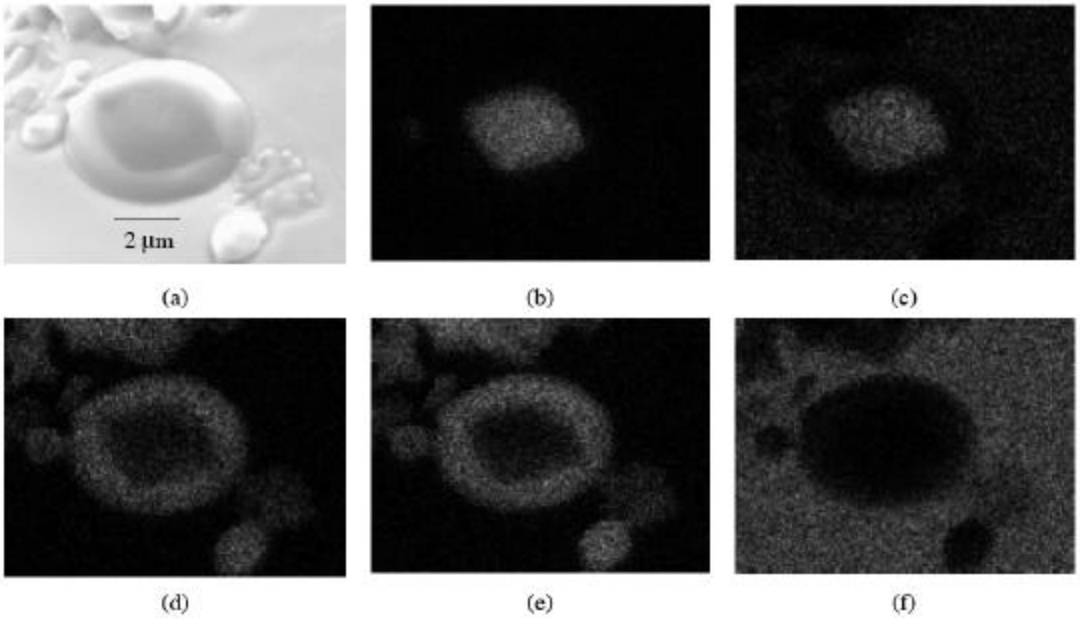

Figure 20: Chemistry of inclusion (a) SEM image, (b) Al, (c) O (d) Ca (e) S (f) Fe.

During solidification, S and Al get rejected into the liquid and raise the potential of CaS precipitation according to:

$$\frac{3-2y}{3x-3y}(CaO)_x \cdot (Al_2O_3)_{1-x} + \frac{2}{3}[Al] + [S] \leftrightarrow \frac{3-2x}{3x-3y}(CaO)_y \cdot (Al_2O_3)_{1-y} + CaS \qquad (12)$$

When this reaction proceeds in the direction of forming solid CaS, it will cause a shape change of the liquid globular Al_2O_3-CaO inclusions by providing them with a solid irregular shell of CaS. The depletion of CaO also leads to an increased crystallization temperature of the Al_2O_3-CaO inclusions. In all the inclusions analyzed in this study, CaO was significantly depleted in the interior of the inclusions.

In summary, the precipitation of CaS and the effect of the same on the evolution of Al_2O_3-CaO inclusions during steel solidification were observed on melt surfaces through CSLM, and showed that:

1. The globular liquid or semi-liquid Al_2O_3-CaO inclusions did not exhibit a trend of agglomeration with each other, even at small separation distance.
2. During solidification, due to the rejection of S and Al from the solid d phase to the melt, the increased melt concentration initiated the reaction between the Al_2O_3-CaO inclusions with the dissolved S and Al, which resulted in the size and shape change of the inclusions, because of the formation of solid dense CaS shells around them.
3. Thermodynamic calculations and solute partitioning estimations suggest that the primary responsible reaction for CaS formation is:

$$9.524(Al_2O_3)_{0.43}\cdot(CaO)_{0.57}+\frac{2}{3}[Al]+[S]\leftrightarrow 8.857(Al_2O_3)_{0.5}\cdot(CaO)_{0.5}+CaS$$

4. The CaS formation rate was observed to increase with the temperature decreasing initially. This temperature dependence suggests the supply of Al and S due to solidification and solute rejection is controlling the rate at early stage, while at the late stage, this growth obeys $Dr \propto \sqrt{t}$, which indicates a diffusion mechanism.
5. After CaS formation and shape change, the inclusions were found to agglomerate due to (i) initially fluid flow and later (ii) capillary depression.

Thus for liquid inclusion removal one must be concerned about the actual condition of an inclusion at the interface. Slag chemistries must be developed that will allow dissolution of any inclusion that appears at the interface, if solid. If liquid, the issue will be one of separation at the interface and refining times are likely to be longer due to this fact. Thus fluid flow patterns in ladles and tundishes must be considered in order to develop inclusion trajectories that will aid in film breakage and enhanced separation efficiency.

This part of the work was awarded the 2003 Marcus A. Grossmann award by ASM for the best paper published in the Journal Materials and Metallurgical Transaction for the year 2003.

Personnel involved in this research

This project has been managed by Assistant Professor Sridhar Seetharaman and Professor Alan W. Cramb. The work has been performed primarily by CIT graduate student Yan Wang who graduated in January 2004 and Martin E. Valdez who was a visiting researcher. Mr. Robert C. Evans has been assisting with different aspects of equipment design, repair and construction.

In addition, several short term visitors and students have been involved in assisting in various specific aspects of the work. These include: A. Gomez, C. Circutti, Prof. Yi, Ms. C. Tse, Dr. H. Shibata, Dr. C. Mutale, S.H. Lee and J.T. Kwon.

References

1. A. W. Cramb: High Purity, Low Residual and Clean Steels
2. H. Itoh: PhD Thesis, Japan, 1996.
3. S. Dimitrov, A. Weyl and D. Janke: Control of the aluminum-oxygen reaction in pure iron melts, Steel Research 66 (1995) No 1, pp. 3-7.
4. D. Janke and A. Fischer: Deoxidation equilibria of titanium, aluminum and zirconium in iron melts at 1600 C, Arch. Eisenhüttenwes. 47 (1976) No 4, pp. 195-198.
5. S. Sridhar and A. W. Cramb: Inclusion Optimization for Next Generation Steel Products, October 2001.

6. M. Valdez et al.: Dissolution of Alumina Particles in CaO-Al2O3-SiO2-MgO Slags.
7. C. Orrling: Crystallization in Slags, PhD Thesis, CMU 2000.
8. R. Rastogi and A. W. Cramb: Inclusion Formation and Agglomeration in Aluminum Killed Steels.
9. G. Li and H. Suito: Effect of Alloying Element M (M = C, Te, Mn, Cr, Si, Ti, Zr, and Ce) on Supersaturation during Aluminium Deoxidation of Fe-Al-M Melts, Metallurgical and Materials Transactions B, Vol. 28B (1997), pp. 259 – 264.
10. The Japan Society for the Promotion of science: 'Steelmaking Data Source Book', revised Edition, Tokyo 1988.
11. W. O. Philbrook: Oxygen reactions with liquid steel, International Metals Reviews, September 1977, pp. 187-201.
12. E. T. Turkdogan: Deoxidation of steel, Journal of the Iron and Steel Institute, January 1972, pp. 21-36.
13. H. Suito, R. inoue and A. Nagatani: Mullite as an electrochemical probe for the determination of low oxygen activity in liquid iron, Steel Research, vol. 63, no 10, 1992, pp. 419-425.
14. R. Inoue and H. Suito: Determination of oxygen in Iron-Aluminum Alloy by inert gas fusion-infrared absorptiometry, Materials Transactions, JIM, vol. 32, no 12, 1991, pp. 1164-1169.
15. K. Tagushi, H. Ono-Nakazato, D. Nakai, T. Usui and K. Marukawa: Deoxidation and Desulfurization Equilibria of Liquid Iron by Calcium, ISIJ International, vol. 43, no 11, 2003, pp. 1705-1709.
16. V. Y. Dashevskii, A. M. Katsnelson, N. N. Makarova, K. V. Grigorovitch and V. I. Kashin: Deoxidation Equilibrium of Manganese and Silicon in Liquid Iron-Nickel Alloys, ISIJ International, vol. 43, no 10, 2003, pp. 1487-1494.
17. H. Ohta and H. Suito: Thermodynamics of Aluminum and Manganese Deoxidation Equilibrian in Fe-Ni and Fe-Cr Alloys, ISIJ International, vol. 43, no 9, 2003, pp. 1301-1308.
18. P. Kozakevitch and L. Lucas, *Revue de Metallurgie*, 65, pp. 589-598 (1968)
19. P. Kozakevitch and Olette, Revue de Metallurgie, 68, pp. 636-646 (1971)
20. P. Kozakevitch and Olette, "Role of surface phenomena in the mechanism of removal of solid inclusions", Production and application of clean steel, Intl. Conference, 1970, Balatonfured, Hungary, The Iron and Steel Institute, London, pp. 42-49
21. P.V. Riboud and M. Olette, "Mechanisms of some of the reactions involved in secondary refining", Proc. 7th International conference on vacuum metallurgy, (1982), Tokyo, Japan, pp. 879-889
22. A.W. Cramb and I. Jimbo, "Interfacial considerations in continuous casting", W.O. Philbrook memorial symposium, Toronto, Ontario Canada, 17th – 20th April (1988), ISS, Inc., pp. 259 – 271, Warrendale, PA, USA
23. S. Hartland: Thin liquid films, fundamentals and applications. Surface Science Series, Vol. 29. Edited by: I.B. Iuvanov, Marcel Dekker Inc., NY 1988
24. D. Bouris and G. Bergeles: *Metallurgical and Materials Transactions B*, **29B**, pp. 641-649 (1998)

25. K. Nakajima and K. Okamura: 4th Intl. Conf. on Molten Slags and Fluxes, ISIJ, Sendai, 1992, pp. 505-510
26. J.W. Cleaver and B. Yates: *J. Coll. Interface Sci*., **44**, pp. 464-474 (1973)
27. A.K. Lahiri, R. Yogambha, P. Dayal and S. Seetharaman: Proceedings of the Mills Symposium (this volume)
28. P. Misra, V. Chevrier, S. Sridhar and A.W. Cramb, "In situ observations at the (Mn,Si)-killed steel/CaO-Al_2O_3 interface", *Metallurgical and Materials Transactions B*, **31B**, pp. 1135-1139 (2000)